


Article

Enhanced Organics Removal Using 3D/GAC/O₃ for N-Containing Organic Pharmaceutical Wastewater: Accounting for Improved Biodegradability and Optimization of Operating Parameters by Response Surface Methodology

Jun Wei Goh ¹, Raphael Jun Hao Tan ¹, Weiyi Wu ² , Zhaohong Huang ², Say Leong Ong ¹  and Jiangyong Hu ^{1,*}

¹ Department of Civil & Environmental Engineering, National University of Singapore, 1 Engineering Drive 2, Singapore 117576, Singapore; say.leong_ong@nus.edu.sg (S.L.O.)

² Singapore Institute of Manufacturing Technology, 2 Fusionopolis Way #08-04 Innovis, Singapore 138634, Singapore; wu_weiyi@simtech.a-star.edu.sg (W.W.)

* Correspondence: hujiangyong@nus.edu.sg

Abstract: Pharmaceutical industry effluents often contain high concentrations of refractory organic solvents, chemical oxygen demand (COD), and total dissolved solids (TDSs). These wastewaters, including N-containing organic solvents known for their persistence and toxicity, pose significant environmental challenges. The study evaluated the efficacy of 3D/Granular Activated Carbon (GAC)/O₃ treatment compared to linear process additions when treating real pharmaceutical wastewater, and revealed a 2.73-fold enhancement in COD mineralization. The process primarily involves the direct oxidation of monoprotic organic acids found in real pharmaceutical effluents, such as acetic and formic acid, crucially influencing mineralization rates. Optimal conditions determined via the response surface methodology were 125 g/L GAC, 30 mA/cm², and 75 mg/L O₃, achieving high total organic carbon (TOC) and COD removal efficiencies of 87.19 ± 0.19% and 89.67 ± 0.32%, respectively (R² > 0.9), during verification runs. Current density emerged as the key parameter for organic abatement, aligning with the emphasis on direct oxidation at the anode surface. This integrated approach enhances biodegradability (BOD₅/COD) and reduces acute toxicity associated with persistent N-containing solvents, demonstrating promising applications in pharmaceutical wastewater treatment.

Keywords: advanced oxidation process; pharmaceutical; electrochemical; 3D; design of experiment (DoE); response surface methodology (RSM)



Citation: Goh, J.W.; Tan, R.J.H.; Wu, W.; Huang, Z.; Ong, S.L.; Hu, J. Enhanced Organics Removal Using 3D/GAC/O₃ for N-Containing Organic Pharmaceutical Wastewater: Accounting for Improved Biodegradability and Optimization of Operating Parameters by Response Surface Methodology. *Water* **2024**, *16*, 3138. <https://doi.org/10.3390/w16213138>

Academic Editor: Alexandre T. Paulino

Received: 11 August 2024
Revised: 27 October 2024
Accepted: 31 October 2024
Published: 2 November 2024



Copyright: © 2024 by the authors. Licensee MDPI, Basel, Switzerland. This article is an open access article distributed under the terms and conditions of the Creative Commons Attribution (CC BY) license (<https://creativecommons.org/licenses/by/4.0/>).

1. Introduction

Pharmaceutical wastewaters are effluents from pharmaceutical production facilities. Pharmaceutical production methods can be categorized into three groups: (1) chemical synthesis, (2) fermentation, and (3) natural product extraction [1]. Typically, these pharmaceutical production procedures are batch-based and multi-step. Despite utilizing the same battery of reactors and separators, the composition and concentration of the wastewater from these pharmaceutical units frequently vary. Reportedly, the amount of waste generated during the production of pharmaceuticals exceeded the quantity of the target product by 50 to 30,000 kg waste/kg of desired product [1,2]. Pharmaceutical wastewaters are frequently described as having elevated chemical oxygen demand (COD), total dissolved solids (TDSs), salinity, toxicity, and refractory solvents [1,3,4], which poses a significant challenge for treatment.

With the extensive use of nitrogen-containing solvents in the processes, pharmaceutical wastewater typically contains elevated levels of nitrogenous chemicals [5]. Toxic concerns are related to nitrogenous organic compounds in pharmaceutical effluent [6,7]. High-saline

pharmaceutical wastewater may also restrict microbial activity due to salinity, presenting a severe biological treatment challenge. This is due to the uneven osmotic potential across the cell wall, which ultimately causes dehydration and death [6,7]. Generally, the BOD₅/COD ratio of reported pharmaceutical wastewaters is <0.5 [1,3] which suggests poor biodegradability. Hybrid technologies combining one or more treatment strategies were recommended to treat recalcitrant and highly concentrated pharmaceutical effluents effectively. Hybrid treatment strategies exist as single-treatment methods (e.g., biological treatment and membrane processes) may not eliminate all pharmaceutical components. It has been demonstrated that coupling adsorption with advanced oxidation processes (AOPs) can improve the overall degradation performance and reduce treatment time and chemical or energy needs [8]. This hybrid approach to treatment can solve the limitations of the different treatment methods. Primarily, AOPs are used to eliminate adsorbed organic contaminants and regenerate adsorbents.

Due to the multiple pathways of •OH synthesis, like catalytic ozonation, peroxone reaction, and O₃-electrolysis, 3D/GAC/O₃ has been presented as an auxiliary approach for the pre- or post-treatment of saline and refractory pharmaceutical wastewater. Three-dimensional (3D) electrochemical advanced oxidation processes (E-AOPs) involve placing conductive particles between the anode and cathode in a traditional electrochemical reactor.

For this study, GAC is used as conductive particles. The prevalence of high salinity and electric conductivity in pharmaceutical wastewaters is the driving force behind the implementation of such E-AOPs [9]. In recent years, similar studies using 3D/GAC/O₃ have been evaluated for pharmaceutical removal [9,10]. However, the degradation process has only been evaluated using a one-factor-at-a-time (OFAT) approach, which may not account for the interacting effects among the independent factors. So, it fails to identify the actual optimal point. Hence, in this study, the 3D/GAC/O₃ has been statistically designed using central composite design (CCD) and response surface methodology (RSM) to arrive at the best combination of operating parameters that give the maximum organic abatement efficiency. The contributions of each abovementioned organics removal mechanism to bulk total organic carbon (TOC) and COD reduction in pharmaceutical wastewater were also assessed in this study. Improved biodegradability and toxicity were similarly observed previously [9,11] but not accounted for. The degradation of the recalcitrant N-containing pharmaceutical organic solvents can be set to explain the improved biodegradability and decrease in toxicity inhibition.

Hence, this study aims to (1) explain the organic mineralization mechanism of 3D/GAC/O₃, (2) demonstrate the use of response surface methodology (RSM) to recommend the optimal conditions for 3D/GAC/O₃, and (3) explain the underlying principles and reasons why biodegradability improved through a detailed analysis of change in the prevalent organic compounds when treating pharmaceutical effluent.

2. Materials and Methods

2.1. Chemicals and Reagents

The chemicals and reagents used in this study are listed in Text S1.

2.2. Pharmaceutical Wastewater Samples

Pharmaceutical wastewater samples were collected from a local pharmaceutical facility in Singapore. The collected samples were stored in polyethylene containers at 4 °C and brought to room temperature prior to usage in experiments and analysis. Table 1 summarizes the characteristics of pharmaceutical wastewater.

Table 1. Characteristics of pharmaceutical wastewater sample.

Parameters	Values
pH	11.30–11.70
Conductivity (mS/m)	84–170

Table 1. Cont.

Parameters	Values
BOD ₅ (mg/L)	27,000–31,200
COD (mg/L)	130,000–210,000
TOC (mg/L)	68,700–90,100
Total Nitrogen (mg/L)	18,800–20,700
Total Alkalinity as CaCO ₃ (mg/L)	43,200–44,600
TDS (mg/L)	85,000–125,000
Cl ⁻ (mg/L)	26,000–45,600
SO ₄ ²⁻ (mg/L)	1200–2000
Na ⁺ (mg/L)	33,100–38,000
NH ₄ ⁺ (mg/L)	2000–2500

2.3. N-Containing Pharmaceutical Organic Solvents

As previously stated, organic solvents are utilized during production, considerably contributing to the effluent being highly concentrated and recalcitrant. With the use of GC/MS, the organic solvents were identified. An AOC-5000 Auto-Injector injected pharmaceutical wastewater sample directly into GC-2010-QP2010 (Shimadzu, Kyoto, Japan). Using a Mega-wax column (High polarity; Length (30 cm) × Diameter (0.25 mm I.D) × Film (0.25 μm)) and a temperature program (Table S1), the spectrum seen in Figure 1 is obtained. Dimethyl-formamide (DMF), Dimethyl-acetamide (DMAc), and acetamide are the most prevalent N-containing amine and amide organic solvents.

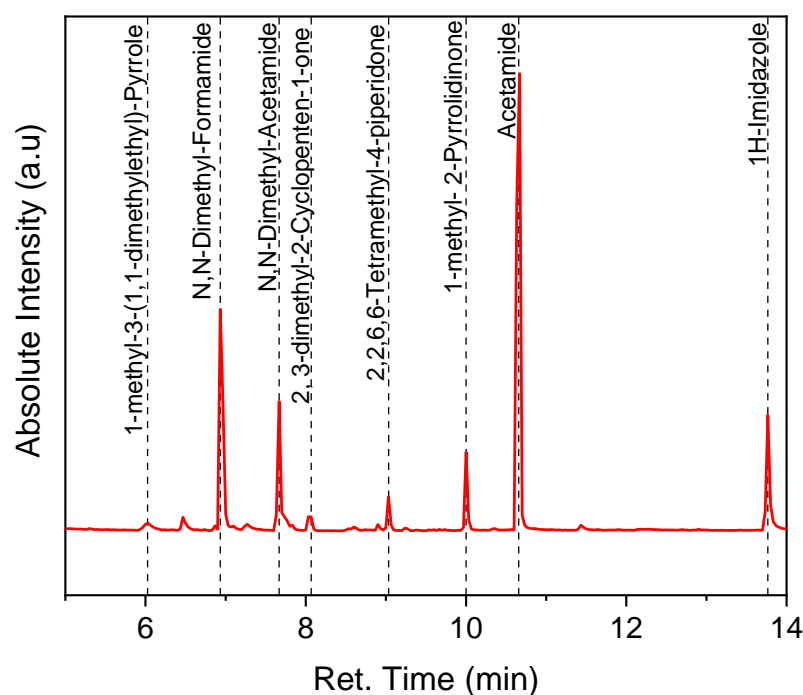


Figure 1. GC/MS chromatogram of pharmaceutical wastewater sample using Mega-wax column (High Polarity).

As detected by the GC/MS spectrum (Figure 1), the N-containing organic solvents can be represented as % area (Figure S1) based on the area beneath each peak. The chemical formulas, molecular weight, Log P, and functional groups of organic solvents can be found in Tables S2 and S3. Functional groups such as pyrrole and imidazole, often known as azoles, are commonly found in natural and synthesized medicinal organics [12]. Piperidine is also reported to be commonly present in pharmaceuticals [13]. 2,2,6,6-Tetramethyl-4-piperidone and 1-methyl-2-Pyrrolidinone have been identified as natural products. Based

on their respective Log P, these nitrogen-containing organic compounds can be hydrophilic or hydrophobic. In general, the organic solvents present in the wastewater are largely low-molecular weight compounds. The high pH of pharmaceutical wastewater can be attributed to alkaline solvents such as 1H-imidazole. The mass spectra are also depicted in Figure S2.

2.4. Electrode Materials

The electrodes used in this study are listed in Text S2.

2.5. The 3D/GAC/O₃ Process

A total of 100 mL of pharmaceutical wastewater was treated in an undivided polycarbonate reactor with a reactor capacity of 12.5 cm × 5 cm × 4 cm and a 4 cm gap between parallel electrodes (Figure 2). The selection of polycarbonate is based on its resistance to O₃. GAC is put between the anode and cathode as a particle electrode. The anode is Nb/BDD (12 cm × 5 cm), and the cathode is stainless steel (12 cm × 5 cm). The procedure was carried out under galvanostatic conditions utilizing a DC power source (Rohde & Schwarz, Munich, Germany). By feeding industrial oxygen (99.9% purity) into an ozone generator (Suez Degremont Technologies, Paris, France), O₃ gas is generated and purged into the reactor. The reaction time was determined to be 6 h.

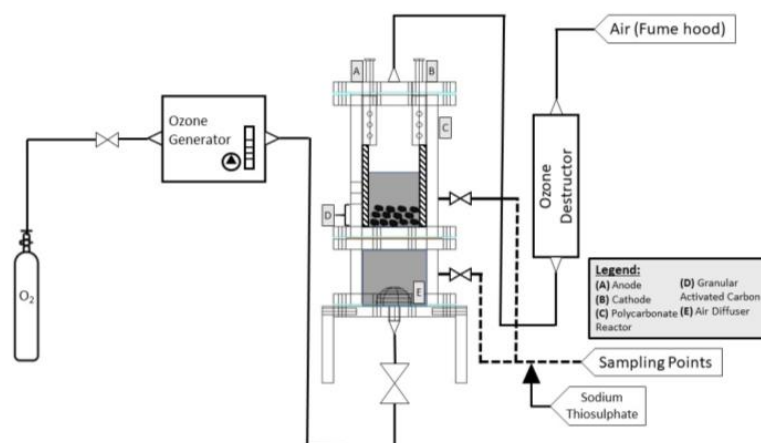


Figure 2. Schematic diagram of 3D/GAC/O₃ electrochemical reactor.

2.6. Electrochemical Characterization

Using an electrochemical workstation (PGSTAT 204, Metrohm Autolab, Utrecht, Netherlands) with a three-electrode cell arrangement, linear sweep voltammetry and cyclic voltammetry (CV) were conducted. The counter and reference electrodes were made of platinum and Ag/AgCl. LSV tests were performed in 0.5 M H₂SO₄ electrolyte with a scan range of 0.0–3.0 V with a scan rate of 50 mVs⁻¹ to assess the anodes' oxygen evolution potential. Tafel plots of the different oxygen evolution reactions (OERs) were determined by converting the observed potentials vs. Ag/AgCl to the reversible hydrogen electrode (RHE) scale using the Nernst Equation (Equation (1)).

$$E_{\text{RHE}} = E_{\text{Ag/AgCl}} + 0.059\text{pH} + E_{\text{Ag/AgCl}}^{\circ} \quad (1)$$

The y-axis of the Tafel graphs represents the OER overpotential (η), which may be calculated by subtracting the thermodynamic potential for OER 1.23 V (vs. SHE) (Equation (2)).

$$\eta = E_{\text{Ag/AgCl}} - 1.23\text{V} \quad (2)$$

In this study, CV experiments were conducted with a scan range of −2.0 to 2.0 V and a scan rate of 50 mVs⁻¹ for three cycles.

2.7. Analytical Method

TOC is determined with the TOC-L analyzer (Shimadzu, Japan). COD and BOD₅ analyses were performed on the pharmaceutical effluent samples according to APHA standard procedure (5220D, 5210B, 1998). COD concentration is measured with a Hach DR 6000 UV-Vis spectrophotometer at 620 nm. Anions and cations were measured by DIONEX ICS-1600 (Thermo Scientific, Waltham, MA, USA) with a DIONEX As-DV (Thermo Scientific, Waltham, MA, USA) autosampler and 930 Compact IC Flex (Metrohm, Utrecht, The Netherlands) with a 919 IC Autosampler, respectively. Toxicity measurements were undertaken using the Microtox[®] method, which suppresses the bioluminescence of the marine bacteria *Vibrio fischeri*. H₂O₂ can be measured by using the Titanium (IV) oxy-sulfate method using a UV-vis spectrophotometer (Hach DR-6000). A yellow complex will be formed upon interaction with H₂O₂, which has an absorbance of 405 nm [14]. Residual dissolved O₃ was determined using the indigo method.

The steady-state concentration of •OH radicals can be measured indirectly using 4-chlorobenzoic acid (pCBA) as a probe molecule across the different reactions of 3D/GAC/O₃. This is especially so with its high reactivity with •OH; $K_{\bullet\text{OH,pCBA}} = 5 \times 10^9 \text{ M}^{-1} \text{ s}^{-1}$ [15].

The rate of degradation of pCBA is given in Equation (3). The integration of Equation (3) yields Equation (4).

$$-\frac{dC_{\text{pCBA}}}{dt} = K_{\bullet\text{OH,pCBA}} C_{\text{pCBA}} C_{\bullet\text{OH}} \quad (3)$$

where C_{pCBA} is the concentration of pCBA and $K_{\bullet\text{OH,pCBA}}$ is $5 \times 10^9 \text{ M}^{-1} \text{ s}^{-1}$.

$$\ln \frac{C_{\text{pCBA}}}{C_{\text{pCBA}_0}} = K_{\bullet\text{OH,pCBA}} C_{\bullet\text{OH}} t \quad (4)$$

$\ln \left(\frac{C_{\text{pCBA}}}{C_{\text{pCBA}_0}} \right)$ was plotted against reaction time on a graph. The slope of the straight lines is equal to $K_{\bullet\text{OH,pCBA}}$ and $C_{\bullet\text{OH}}$ multiplied together. With the known value of $K_{\bullet\text{OH,pCBA}}$, the pseudo-steady state •OH concentration can be calculated. pCBA is also known to have poor adsorption kinetics with activated carbon [16] and low reactivity with O₃ [$k_{\text{O}_3} = 0.15 \text{ M}^{-1} \text{ s}^{-1}$] [17]. It is, therefore, ideal for this study. In total, 0.5 M of pCBA was added to a sample of pharmaceutical effluent, which was then treated using different processes. pCBA was determined using LC-MS/MS (Shimadzu 8030, Japan) using methanol/water (95% v/5% v) with a simple binary gradient for chromatographic separation and a Shim-pack FC-ODS column (150 × 2 mm, particle size 3 μm) at 40 °C.

2.8. Design of 3D/GAC/O₃ by Response Surface Methodology

The 3D/GAC/O₃ is constructed using statistical methods with independent variables, namely, O₃ concentration, GAC dosage and current density, TOC removal efficiency (%), and COD removal efficiency (%) as the dependent variables. The response surface approach is an empirical modeling technique that establishes a link between controlled factors and observable outputs [18,19]. In RSM, central composite design (CCD) and Box–Behnken design (BBD) are the most frequently employed 2nd order regression models [20]. In this study, a central composite design was employed. The optimization entails observing the response of the statistically planned experiment set, determining the coefficients by fitting the experimental data to the functions, predicting the response, and evaluating the model's adequacy. In Table 2, the independent variables are shown. The designations for low, middle, and high levels are −1, 0, and +1, respectively. TOC and COD removal efficiencies are the dependent variables. A total of 40 experiments were conducted to examine the effects of the three variables on organics removal effectiveness.

Table 2. Experimental design levels of dependent variables.

Factor	Variable	Level		
		−1	0	1
X ₁	GAC Dosage (g/L)	50	100	200
X ₂	Current Density (mA/cm ²)	15	30	45
X ₃	Ozone Dosage (mg/L)	30	80	120

Utilizing the coefficient of determination (R^2), Pareto analysis of variance (ANOVA), and statistical and response plots, the findings were evaluated. The experimental data were fitted into a polynomial of the 2nd order using a non-linear regression technique in order to determine the coefficients. The quadratic response model can be described by Equation (5).

$$Y = \beta_o + \sum \beta_i X_i + \sum \beta_{ii} X_{ii}^2 + \sum \beta_{ij} X_i X_j + \varepsilon \quad (5)$$

where β_o is the offset term, β_i is the slope of the input variable, β_{ij} is the quadratic effect of the input variable, and β_{ij} is the linear interaction effect between the various input variables [21].

2.9. Non-Linear Fitting (Adsorption Models)

This study will employ non-linear fitting as it is a direct method for fitting experimental data to theoretical adsorption models. This is only possible with the correct initial parameters and a theoretical model. The parameters can be determined through iterative optimization. The non-linear model fit was accomplished with Origin 2019b.

3. Results and Discussion

3.1. The 3D/GAC/O₃ Process for Pharmaceutical Wastewater Treatment

3.1.1. Electrochemical Characterization of BDD with Pharmaceutical Wastewater

On the BDD, cyclic voltammetry and liner sweeping voltammetry tests were conducted with various matrices, including wastewater samples and electrolytes such as Na₂SO₄ and NaCl. Compared to the electrolytes of 0.1 M Na₂SO₄ and 0.2 M NaCl, there is evidence of a slight anodic peak for CSV and a change in the current before OEP (Figure 3). According to the scientific literature, it is likely related to chlorine evolution reaction (CER) [22].

3.1.2. Comparison Between Processes on Organics Removal

As shown in Figure 4 and Table S6, the combined 3D/GAC/O₃ process ($k_{\text{COD}} = 8.146 \times 10^{-5} \text{ s}^{-1}$) has a synergistic factor of 2.73 when compared to the linear combination of its processes of O₃, GAC, and electro-oxidation ($k_{\text{COD}} = 0.395 \times 10^{-5} \text{ s}^{-1}$, $1.187 \times 10^{-5} \text{ s}^{-1}$, and $0.602 \times 10^{-5} \text{ s}^{-1}$, respectively). O₃-Electrolysis ($k_{\text{COD}} = 5.70 \times 10^{-5} \text{ s}^{-1}$), 3D electro-oxidation ($k_{\text{COD}} = 2.77 \times 10^{-5} \text{ s}^{-1}$), and catalytic ozonation ($k_{\text{COD}} = 4.589 \times 10^{-5} \text{ s}^{-1}$) exhibit the respective synergistic factors of 4.717, 0.550, and 1.900 when compared to their respective individual processes. Similar observations were reported with TOC removal, with the observed rate constants for 3D/GAC/O₃ ($k_{\text{TOC}} = 7.328 \times 10^{-5} \text{ s}^{-1}$) being approximately ~81% greater than the linear sum of the rate constants for ozonation ($k_{\text{TOC}} = 0.441 \times 10^{-5} \text{ s}^{-1}$) and 3D electro-oxidation ($k_{\text{TOC}} = 3.607 \times 10^{-5} \text{ s}^{-1}$) (Table S6). The synergistic factor is calculated using Equation (S1).

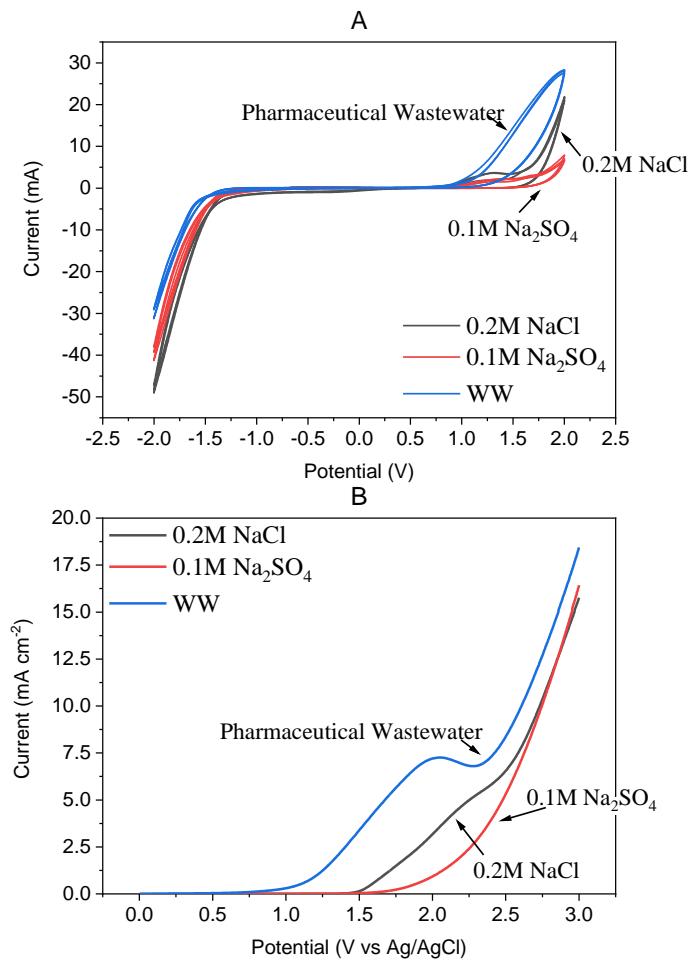


Figure 3. (A) CSV and (B) LSV of BBD in various matrices of 0.2 M NaCl, 0.1 M Na₂SO₄, and pharmaceutical wastewater at the scan rate of 50 mVs⁻¹.

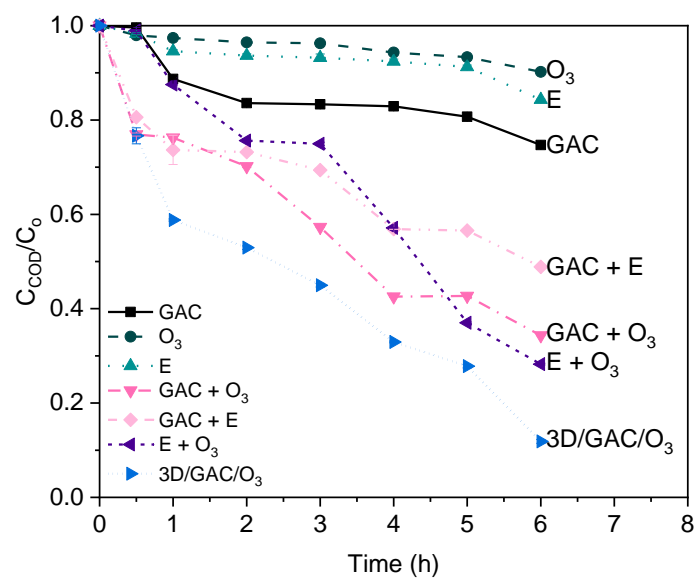


Figure 4. C_{COD}/C_o against time (h) for different treatment processes.

The order of mineralization is comparable to that seen in a different study using 3D/GAC/O₃ to mineralize nitrobenzene [10]. The increase in mineralization is likely a result of the additive generation of •OH radicals by various processes.

3.2. Determining the $\bullet\text{OH}$ Production and Reactions in 3D/GAC/O₃

As noted in Table S7, the measured rate constant for 3D/GAC/O₃ ($k_{\text{pCBA}} = 26.45 \times 10^{-4} \text{ s}^{-1}$) is ~188% greater than the linear sum of the reaction rate constants for the separate processes. The [OH]_{ss} of 3D/GAC/O₃ is approximately 21% more than the [OH]_{ss} produced by catalytic ozonation and electro-oxidation separately ($37.21 \times 10^{-14} \text{ M}$ and $6.563 \times 10^{-14} \text{ M}$).

The order of $\bullet\text{OH}$ production is shown in Table S7 and Figure 5: 3D/GAC/O₃ > GAC/O₃ > E/O₃ > E/GAC > GAC > E > O₃ which differs from the order of mineralization determined previously, 3D/GAC/O₃ > E/O₃ > GAC/O₃ > GAC/E > GAC > E > O₃. The difference is due to the formation of short-chain organic acids, which are more resistant to oxidation by $\bullet\text{OH}$ radicals than to direct oxidation [23]. It has also been suggested that BDD is responsible for the direct anodic oxidation of these simple carboxylic acids [11]. This causes the mineralization rate to be highly dependent on direct electron transfer oxidation processes, which explains the disparity between organic abatement and $\bullet\text{OH}$ generation. In addition, BDD anodes exhibit exceptional electrochemical characteristics for electron transfer processes and direct oxidation [24,25].

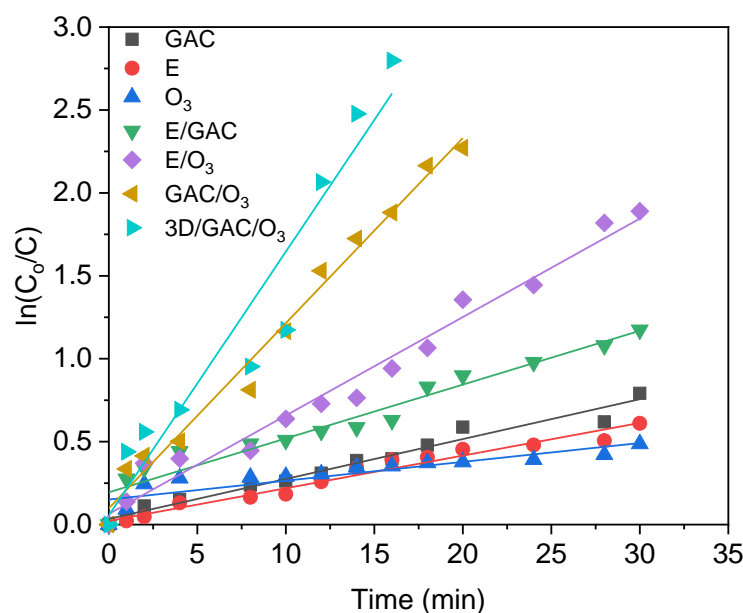


Figure 5. $\ln(\text{pCBA}/\text{pCBA}_0)$ against time due to various treatment processes. 50 M pCBA spiked into pharmaceutical wastewater sample.

3.3. Reactions Contributing to the Generation of $\bullet\text{OH}$ for 3D/GAC/O₃

3.3.1. Peroxone Reaction

Similar electrochemical processes [9,10,26] have been reported to produce H_2O_2 in other investigations, including research with the same setup as this one (anode: BDD and cathode: stainless steel). Due to the hue of the pharmaceutical wastewater sample, the colorimetric method cannot be used to measure H_2O_2 concentration. Figure S5 depicts how comparable experimental conditions were applied to the 0.1 M Na_2SO_4 electrolyte to determine the generation of H_2O_2 . Similarly to previous findings [9,10], no H_2O_2 was discovered in the 3D/GAC/O₃ process due to the quick reaction of H_2O_2 with O_3 , where $k(\text{HO}_2^- + \text{O}_3) = 9.6 \times 10^6 \text{ M}^{-1} \text{ s}^{-1}$. The TOC and COD removal efficiencies rise from 59% and 51% for 3D/GAC to 72% and 55% for 3D/GAC/O₂ when O_2 is being sparged into the reactor. The subsequent increase in the TOC and COD removal efficiency when 80 mg/L O_3 is sparged into the reactor can be attributed to the increased generation of $\bullet\text{OH}$ radicals by the peroxone process.

3.3.2. Catalytic Ozonation

In accordance with Equations (6) and (7), H_2O_2 can be activated by an activated carbon surface to generate $\bullet\text{OH}$ radicals [27]. The reaction between H_2O_2 and GAC is significantly slower than the reaction between H_2O_2 and peroxone ($k_{\bullet\text{OH}} = 3 \times 10^{-2} \text{ M}^{-1} \text{ s}^{-1}$).



For such heterogeneous catalytic reactions, the primary source of $\bullet\text{OH}$ radicals is hence the interaction between GAC and ozone.

3.3.3. O_3 -Electrolysis

In contrast to carbon-based cathodes, no H_2O_2 is reportedly detected when stainless steel is used as the cathode [28]. H_2O_2 contribution is negligible for 3D/GAC/ O_3 , mainly when an inert metal cathode is utilized [10]. Therefore, O_3 -electrolysis is more likely to occur on the cathode than electro-peroxone. In addition, residual O_3 was not detected despite the sparging of O_3 at such high concentrations since it is heavily consumed by processes such as cathodic reduction, catalytic ozonation, and the direct oxidation of organic compounds and other components of pharmaceutical effluent.

3.4. Model Development, Regression and Variance Analysis, and Optimization

Using the results of the experimental design, Equations (8) and (9) represent the regression equations for TOC removal efficiency % and COD removal efficiency %, respectively.

$$\text{TOC Removal Efficiency (\%)} = -14.77 + 0.4036X_1 + 1.081X_2 + 1.1187X_3 - 0.000917 X_1^2 + 0.00852X_2^2 - 0.005835X_3^2 - 0.002189X_1X_2 + 0.000275X_1X_3 - 0.008538X_2X_3 \quad (8)$$

$$\text{COD Removal Efficiency (\%)} = -37.37 + 0.4327X_1 - 0.219X_2 + 2.123X_3 - 0.000640X_1^2 + 0.02765X_2^2 - 0.012606X_3^2 - 0.003384X_1X_2 - 0.000599X_1X_3 - 0.00239X_2X_3 \quad (9)$$

In this investigation, the model F values for the TOC removal efficiency (%) and COD removal efficiency (%) were 94.19 and 69.8, whereas the p -values were less than 0.0001. As shown in Tables S8 and S9, this suggests that the models obtained for both surrogate parameters were significant. Figures S6A and S7A demonstrate that the anticipated values of the model response are highly associated with the observed values, with R^2 values of 0.9672 and 0.95352, respectively. Model appropriateness may also be determined using determination coefficient values (R^2). The regression coefficients (R^2) for the TOC removal efficiency (%) and COD removal efficiency (%) were calculated to be 0.9658 and 0.9544, respectively. This demonstrated the model's overall accuracy in predicting the values (Table S10). As demonstrated in Tables S8 and S9, the lack-of-fit values for both models are not statistically significant ($p > 0.05$), supporting the validity of the quadratic regression models. The surface response and contour plots for both TOC and COD reduction can be observed in Figures 6 and S8–S10.

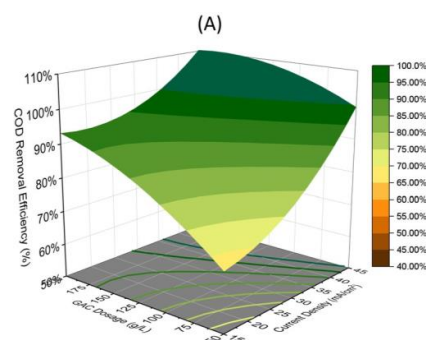


Figure 6. Cont.

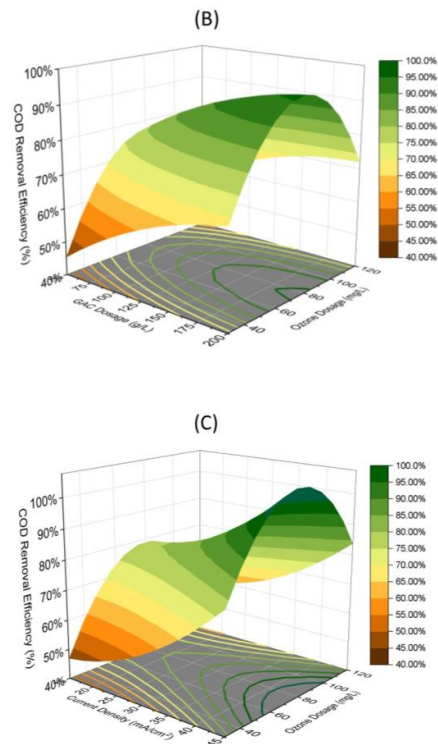


Figure 6. Three-dimensional surfaces of the interaction of independent variables: (A) for GAC and current density, (B) for GAC and ozone, and (C) for current density and ozone in terms of COD removal efficiency (%).

3.4.1. Influence of Single Variables

As demonstrated in Figure 7A–C, the primary effects of the variables can be evaluated. The contours of the three variables for the TOC and COD removal main effects plots are identical. Both the GAC dose (X_1) and current density (X_2) have a positive influence on the organic abatement efficiencies.

The effect of the GAC dose suggests that organic abatement efficiencies plateau despite the increased number of active sites offered by a higher GAC dosage. This is because the limiting factor is the solubility of O_3 in aqueous solution for catalytic ozonation. This is also attributable to both the ongoing adsorption and rapid production of $\bullet OH$ due to catalytic ozonation before the efficiency of activated carbon decreases significantly as pyrrole groups are depleted by continuous O_3 sparging [29].

Due to its direct engagement in organic abatement, the effect of current density on both TOC and COD rose rapidly. This is likely owing to the increased $\bullet OH$ generation through the more prevalent pathway of O_3 -electrolysis when the increase in current density causes a greater degree of O_3 reduction to generate more $\bullet OH$ [30–32]. With the presence of chloride, it is also likely that more active chlorine is produced, which may aid in the total breakdown of the pharmaceutical organics [9,33,34]. It is also possible that the increase in current density increases the rate of the direct oxidation of carboxylic acids on the anode surface, which has proven to be crucial for the complete mineralization of pharmaceutical organics due to the presence of carboxylic acids.

O_3 can function as a direct oxidant or produce homogeneous $\bullet OH$ via O_3 -electrolysis, catalytic ozonation, or peroxone with H_2O_2 produced by polarized GAC. According to mass transfer theories, raising the O_3 concentration in the gas phase would significantly enhance the rate of O_3 mass transfer to the aqueous phase. Hence, raising the sparged O_3 concentration will increase the formation of $\bullet OH$ radicals due to the mechanisms mentioned previously, and more O_3 would be available to degrade the O_3 -compatible pharmaceutical organic solvents. The abatement reaching a plateau at increased O_3 concentration is comparable to another work [10] with O_3 -electrolysis being the dominant pathway for

•OH generation. Beyond a critical point of O₃ dosage (Figure 7C), there is a drop in organic abatement. This is because O₃ is reduced preferentially over O₂ on the cathodic side of the polarized GAC. This causes an inhibition of O₂ reduction to H₂O₂ when the O₃ concentration exceeds a certain threshold [35]. Peroxone reaction produces fewer •OH radicals, resulting in a decline in organic abatement. This was explored and seen in a study with identical objectives [9].

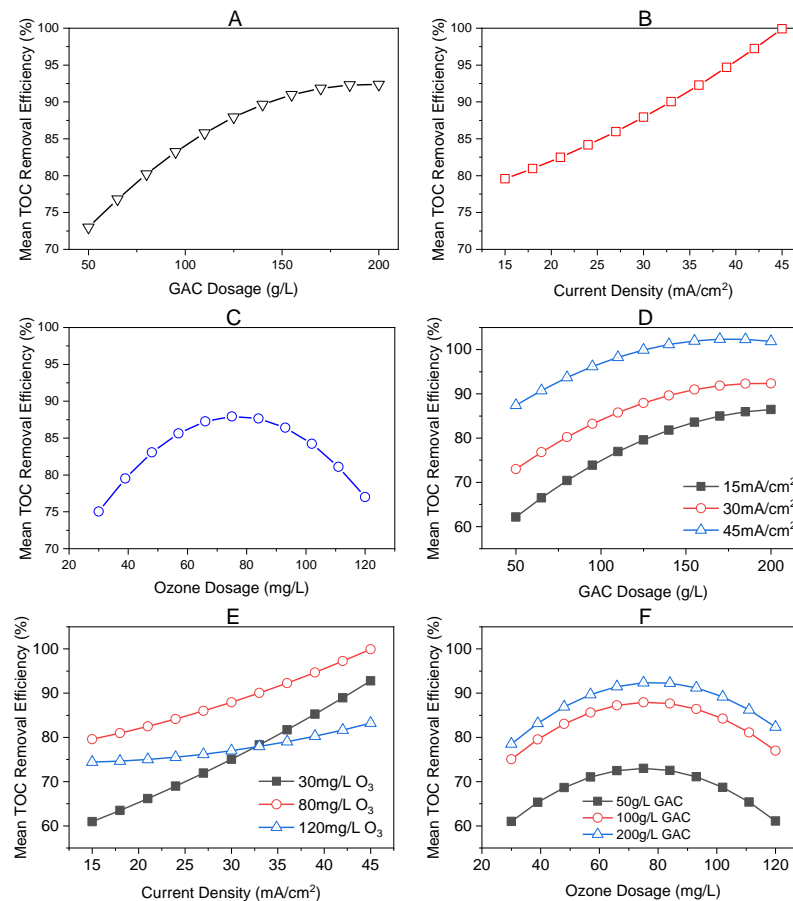


Figure 7. Main effects plot for TOC removal efficiency (%): (A) GAC dosage, (B) current density, and (C) ozone dosage; main effects plot for TOC removal efficiency (%): (D) GAC dosage, (E) current density, and (F) ozone dosage.

3.4.2. Interaction between Variables

Similar observations and conclusions can be drawn from the main effects plots and analysis of independent components, as depicted in Figure 7D–F. The crossing lines found in Figure 7E indicate a crucial amount of interaction for the overall response (organic abatement). It comes as no surprise that these two variables interact. Combining these two variables (O₃-electrolysis) is the process that contributes the most in terms of organic abatement to 3D/GAC/O₃.

3.4.3. Pareto Analysis

A graphical Pareto analysis can be used to illustrate the effect of independent variables on the response [36]. As illustrated, the Pareto analysis can be stated as Equation (10).

$$P_i = \frac{b_i^2}{\sum_i b_i^2} \times 100 \quad (i \neq 0) \quad (10)$$

where b_i refers to the numerical coefficient effect of each parameter.

According to the Pareto chart (Figure S11), current density (X_2) is the most influential parameter for organic removal utilizing the 3D/GAC/O₃ method. This is consistent with the preceding explanation in an earlier section, which stated that the mineralization rate mainly depends on the direct oxidation of carboxylic acids on the anode surface. The influence of current density is one of the most significant factors for both TOC and COD models, with F-values of 292.64 and 182.73 ($p < 0.001$) compared to X_1 and X_3 . The current density (X_2), the factor with the most significant effect on the overall organic removal, is consistent with prior research that applied both DoE and E-AOP treatment for pharmaceutical wastewater [33,37] (Tables S8 and S9).

3.4.4. Optimization of Parameters

As the model fails to identify the top limit boundary of 100% removal efficiency, the optimal condition to maximize the removal efficiencies for TOC and COD is projected with the boundary condition specified. The optimal conditions comprised 125 g/L GAC, 30 mA/cm², and 75 mg/L O₃. Under optimal conditions, the verification run yielded the TOC and COD removal efficiencies of $87.19 \pm 0.19\%$ and $89.67 \pm 0.32\%$, respectively. The removal efficiencies fell within the confidence and prediction interval of the projected response with 95% confidence. To fit the experimental data, the pseudo-first-order kinetics model was utilized, and the kinetic equations are provided in Equation (11).

$$n\left(\frac{C_o}{C_t}\right) = \begin{cases} 0.31562 \tau, & \text{Total Organic Carbon (TOC)} \\ 0.32192 \tau, & \text{Chemical Oxygen Demand (COD)} \end{cases} \quad (11)$$

C_o : Initial Surrogate Organic Concentration, C_t : Surrogate Organic Concentration at given time (t)

The experimental data were consistent with a pseudo-first-order kinetics model with a linear connection between $\ln(C_o/C_t)$ and time (Figure S12). TOC and COD degradation had the respective rate constants of 0.31562 h^{-1} ($R^2 = 0.96862$) and 0.32192 h^{-1} ($R^2 = 0.97171$) (Table S11).

3.5. Degradation and Changes of Amides and Imides

As noted in Figure S13 and Table S12, N-methyl-formamide (NMF), and formamide are formed. These organic solvents are known byproducts of DMF, which have been proposed in previous research [38–40]. Figure S14 illustrates the suggested degradation process of DMF by 3D/GAC/O₃ in pharmaceutical wastewater based on the hypothesized breakdown product detected by GC/MS and other published materials. Figure S15 illustrates the GC/MS identification of the organic byproducts of DMF, including NMF and formamide, using their respective mass spectra (Figure S16).

NO₃[−] and NH₄⁺ are released from the decomposition of N-containing organics as previously reported [11] and the same is found in this study. According to the degradation routes of DMF and DMAc, these nitrogenous inorganic ions result from the breakdown of DMF and DMAc (Figures S14 and S17). Comparisons were made between 3D/GAC/O₃, GAC/O₃, and electrolysis oxidation to illustrate the differences in degradation profiles caused by an oxidative environment with increasing intensity.

As demonstrated in Figure 8A,B (3D/GAC/O₃), Figure 8C,D (GAC/O₃), and Figure 8E,F (E), when the oxidative power of the treatment declines, there is a greater buildup of NMF and formamide and a commensurate drop in NO₃[−] production. The oxidative potential of the processes in this instance is as follows: 3D/GAC/O₃ > GAC/O₃ > E, based on their organic abatement efficiency. DMF and DMAc deteriorated during electrolysis oxidation at a slower rate than GAC/O₃ and 3D/GAC/O₃. The additional contribution of formamide, as seen in Figure 8E, can be because formamide is also the ultimate byproduct of 1H-Imidazole [12]. These degradation and transformation characteristics of amides and imides are also indicative of an increase in hydroxyl radical generation.

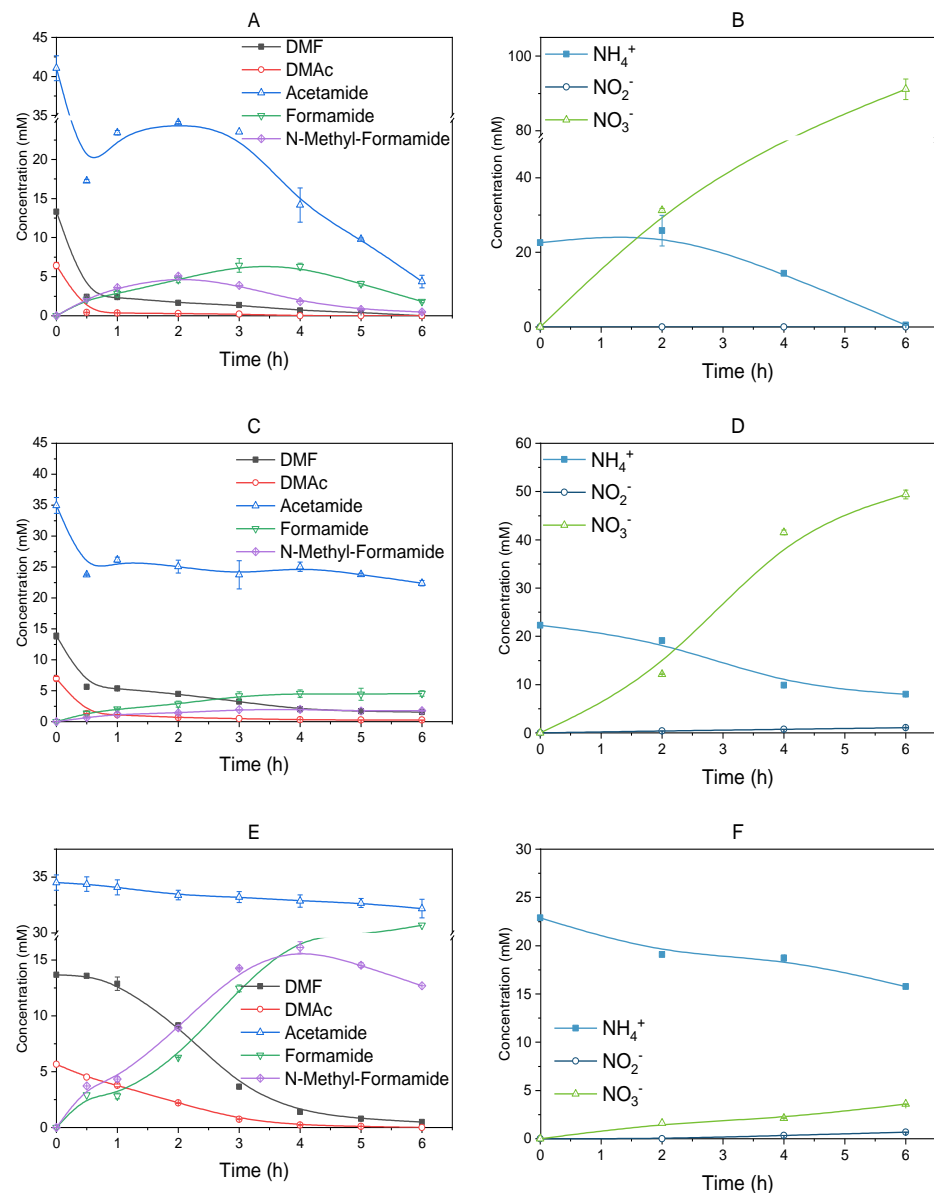


Figure 8. (A) Amide and imide organic constituents and (B) N-inorganic byproducts during 3D/GAC/O₃; (C) amide and imide organic constituents and (D) N-inorganic byproducts during GAC/O₃; (E) amide and imide organic constituents and (F) N-inorganic byproducts during electrolysis oxidation.

3.6. Biodegradability and Toxicity Between Different Processes

The BOD₅/COD ratio of the wastewater is between 0.169 and 0.233, which is below the biological treatment threshold of 0.4. As oxidative processes were introduced, biodegradability increased, reaching 0.86 for BOD₅/COD and 12.38% inhibition after being treated with the 3D/GAC/O₃ process (Figure 9A,B). Figure S18 depicts the general trend of increasing biodegradability and decreasing toxicity inhibition when plotted against COD removal efficiency (%). A similar investigation found a reduction in toxicity inhibition [9].

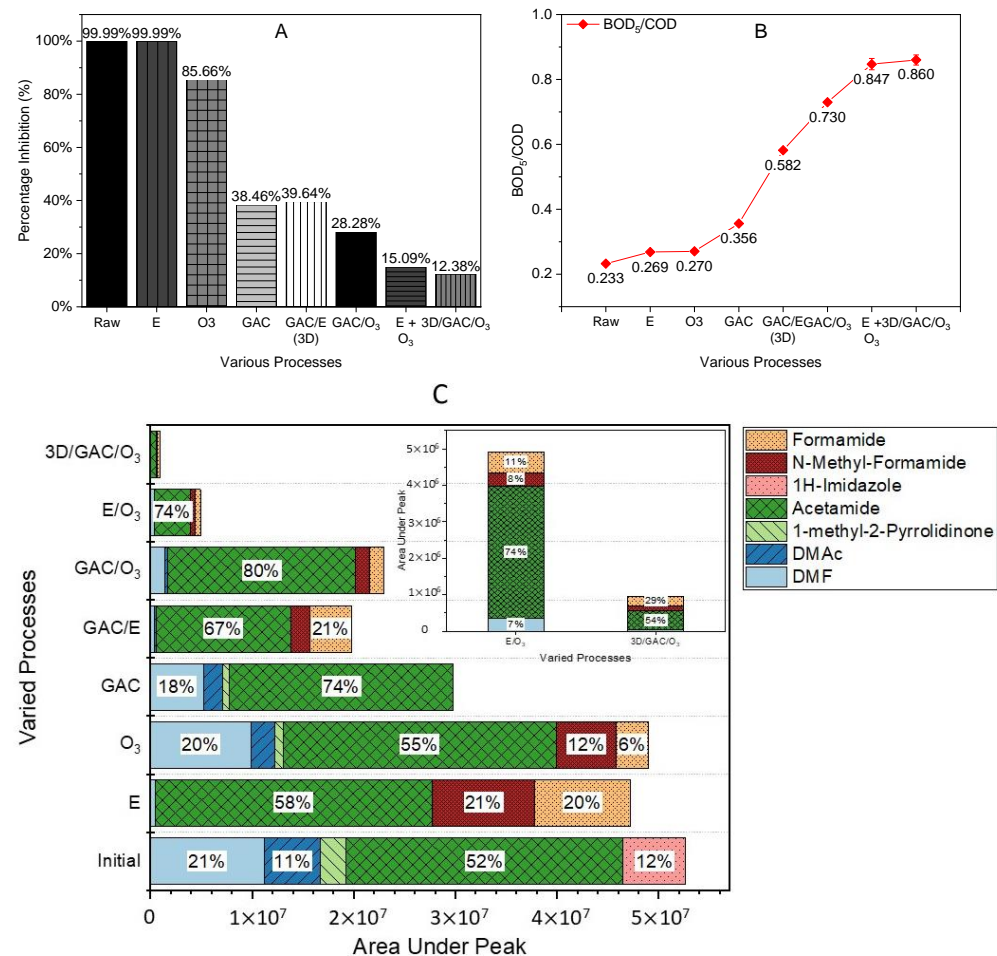


Figure 9. (A) Changes in acute toxicity (2% basic test); (B) BOD₅/COD ratio due to different treatment processes; (C) composition of dominant organic solvents due to various processes (%); Area under Peak.

It has been stated that pharmaceutical wastewater is hardly biodegradable and carries toxicity risks due to nitrogen-containing pharmaceutical organic solvents. Determining which N-containing organics are accountable for the aforementioned properties and the observation made in Figure 9A,B is important. Common pharmaceutical organic solvents like DMF, DMAC, and acetamide are responsible for low biodegradability and high toxicity [41–44]. DMF and DMAC are toxic aprotic polar solvents [45], whereas acetamide is an extremely toxic mutagenic compound [44]. Both the DBA and the European Union have judged them undesirable, classifying them as class 2 solvents [46] and organics of high concern, respectively [47]. As indicated in Table S13 [48], the dominating organic solvents DMF and DMAC were reported to have BOD₅/COD of 0.01.

However, with electrolysis oxidation (E), even if the majority of resistant organic solvents such as DMF and DMAC have been destroyed, the wastewater sample still possesses low biodegradability (BOD₅/COD = 0.269) and strong toxicity inhibition (>99%). This is because formamide and NMF have accumulated (Figure 9C). As shown in Table S13, formamide and NMF have poor degradability with BOD₅/COD values of 0.01 and 0.02, respectively [48]. Both chemicals are reported to be harmful, resulting in deformed zebrafish embryos [49] and severe hepatotoxicity in mice [50]. It has been found that NMF is more hepatotoxic than DMF [51,52] and more toxic than formamide [53].

When 2 g/L of DMF was subjected to adsorption by GAC, ozonation, and electrolysis oxidation, this study demonstrated that the toxicity of DMF's byproducts increased. As illustrated in Figure S19, the formation of byproducts has counterintuitively increased

toxicity. This increase in toxicity due to the formation of byproducts was also discussed in the cited literature [54], as shown in Table S13, with NMF and formamide requiring a lower dose than their parent compound DMF to be considered mouse-lethal.

3.7. Organic Fractions Between Different Processes

As seen in Figure 10A, the treatment methods, except E and GAC, produce LMW acids. The LMW acids, which include acetic and formic acid, are monoprotic organic acids [55]. It has been established that they are the byproducts of dominating N-containing solvents such as DMac and DMF. The existence of these carboxylic acids as a result of the E-AOP treatment of pharmaceutical wastewater has been documented previously [11]. The significant decrease in pH after 6 h of treatment can also be used to confirm the existence of carboxylic acids. The pH of O₃, GAC/E, GAC/O₃, E/O₃, and 3D/GAC/O₃ were 6.27 pH, 8.02 pH, 7.64 pH, and 8.85 pH, respectively, compared to the starting pH of 11.58 pH. Such a decrease in pH was also accounted for while treating pharmaceutical wastewater [9].

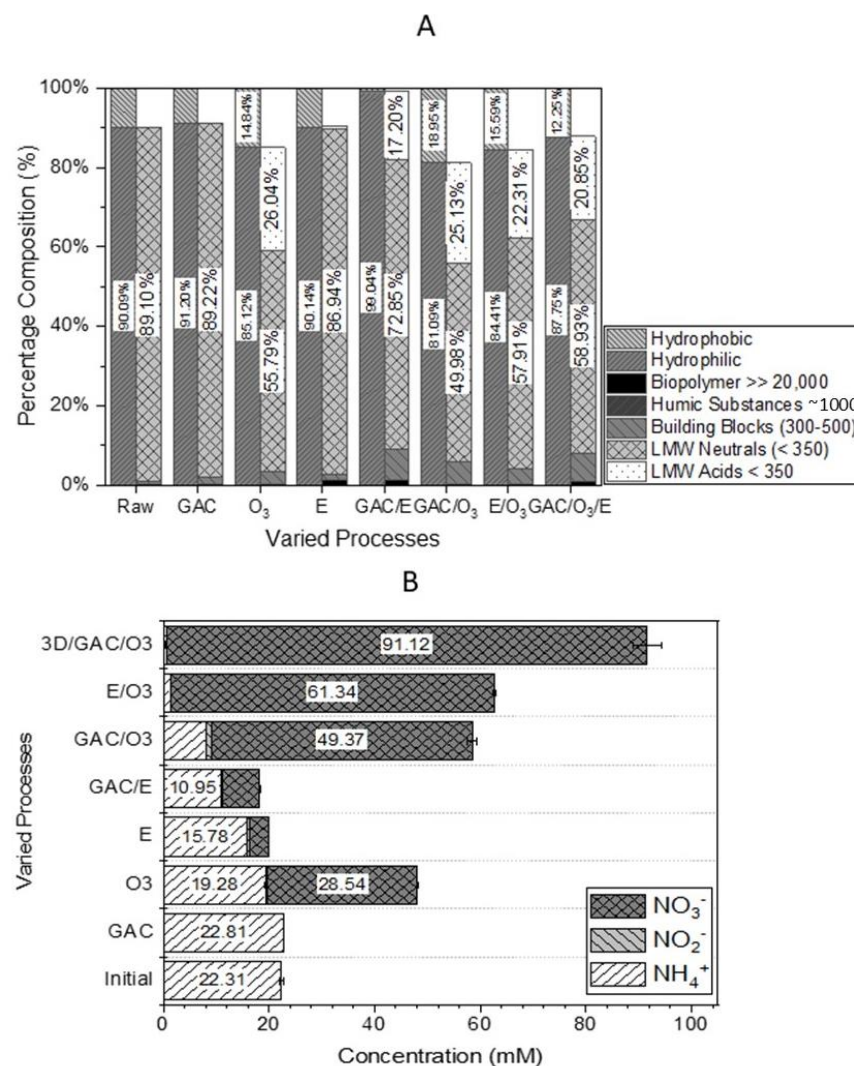


Figure 10. (A) Normalized percentage (%) with respect to DOC of organic fractions including hydrophilic and hydrophobic organic compounds, biopolymers, building blocks, LMW neutrals, and LMW acids due to various treatment processes. (B) Evolution of nitrogenous inorganic ions like NH₄⁺, NO₂⁻, and NO₃⁻ due to various treatment processes.

The more extensive molecular weight distribution of hydrophilic compounds (Figure 10A), accompanied by traces of hydrophobic chemical compounds (e.g., 1-methyl-3-(1,1-dimethylethyl)-Pyrrole), reflects the more substantial occurrence of hydrophilic organic

compounds (Table S2). Biopolymers with a molecular weight of >20,000 have been accounted for in earlier research as potentially being monoclonal antibodies, protein APIs, excipients, and packaging waste materials with a molecular weight of >50,000 Da [1,11,56].

As evidenced by the breakdown paths of the major solvents, such as DMF and DMAc (Figures S12 and S15), carboxylic acids and nitrogenous inorganic ions will be released synchronously. In an oxidative environment, it is, therefore, not surprising that the accumulation of LMW acids will accompany the generation of NO_3^- . This is evident for processes such as 3D/GAC/O₃, E/O₃, GAC/O₃, and O₃ in which $[\text{NO}_3^-]$ generated > $[\text{NH}_4^+]$ present initially as seen in Figure 10B. However, while GAC/E had a greater organic abatement than E, GAC, and O₃, it did not produce an abundance of nitrogenous inorganic ions like the other processes. This may be because GAC adsorbs the byproducts of N-containing solvents predominately. Consequently, this indicates that adsorption remains the primary mechanism for organic abatement in the E/GAC process.

4. Conclusions

This study further substantiated previous work in the compatibility and synergistic degradation capability of 3D/GAC/O₃ treating pharmaceutical wastewater ($k_{\text{COD}} = 8.146 \times 10^{-5} \text{ s}^{-1}$) with a synergistic factor of 2.730 when compared to the linear addition of its processes. The results obtained in the present study demonstrated that while 3D/GAC/O₃ results in multiple pathways of $\bullet\text{OH}$ formation, the mineralization rate predominantly depends on the direct oxidation of monoprotic organic acids (e.g., acetic and formic acid). The optimal conditions determined via response surface methodology were 125 g/L GAC, 30 mA/cm², and 75 mg/L O₃, achieving high total organic carbon (TOC) and COD removal efficiencies of $87.19 \pm 0.19\%$ and $89.67 \pm 0.32\%$, respectively ($R^2 > 0.9$), during verification runs. After being treated by 3D/GAC/O₃, biodegradability reached 0.860 for BOD₅/COD and only 12.38% acute toxicity inhibition. The enhanced biodegradability (BOD₅/COD) and decreased acute toxicity are attributable to the degradation of refractory and toxic N-containing pharmaceutical solvents. Electro-oxidation exposes the accumulation of intermediates (e.g., NMF and formamide) that are more hazardous than their parent chemical. This emphasizes the significance of a strong oxidative environment like 3D/GAC/O₃ for treating highly concentrated pharmaceutical wastewater. The 3D/GAC/O₃ is in its infancy and needs to be evaluated as a viable treatment approach for wastewater treatment. However, this study's findings can be significant concerning future research and development when 3D/GAC/O₃ can be utilized for other similar types of wastewater like tannery, petrochemical, and food processing industries effluents.

Supplementary Materials: The following supporting information can be downloaded at <https://www.mdpi.com/article/10.3390/w16213138/s1>, Text S1. Chemicals And reagents; Text S2. Electrode materials; Table S1. GC/MS temperature program (Mega-Wax); Table S2. Molecular weight, Log P, and functional groups of organic solvents; Table S3. Residence time, structure, and chemical formulae of N-containing pharmaceutical organic solvents; Table S4. Adsorption kinetics model parameters for GAC adsorption of pharmaceutical wastewater; Table S5. Adsorption isotherm parameters in terms of TOC for acetamide, DMAc, and DMF; Table S6. Pseudo 1st-order constants and R^2 for TOC and COD mineralization for different treatment processes; Table S7. Pseudo 1st-order rate constants for pCBA/ $\bullet\text{OH}$, R^2 , and $[\bullet\text{OH}]_{\text{ss}}$ for different treatment processes; Table S8. ANOVA results for TOC removal efficiency (%) for 3D/GAC/O₃; Table S9. ANOVA results for COD removal efficiency (%) for 3D/GAC/O₃; Table S10. Quadratic model summary statistics and quality for TOC% and COD% by 3D/GAC/O₃, Table S11. Multiple response prediction for TOC and COD removal efficiency (%); Table S12. N-organic solvents identified in pharmaceutical wastewater for different treatment processes; Table S13. Organic solvent acute toxicity (LD50) and BOD5/COD; Figure S1. Area % of organic solvents identified for pharmaceutical wastewater; Figure S2. GC/MS mass spectra of organic solvents identified in pharmaceutical wastewater; Figure S3. Adsorption rate (qt) using 100 g/L GAC with pharmaceutical wastewater; Figure S4. (A) Freundlich adsorption isotherm of acetamide, DMAc, and DMF, and Langmuir adsorption isotherm of (B) DMAc (C) acetamide, and (D) DMF in terms of TOC; Figure S5. H₂O₂ production during 3D/GAC/O₃ and 3D/GAC/O₂ processes with reaction

conditions: 100 g/L, 0.1M Na₂SO₄, 30 mA/cm², 0.1 L/min O₂, and O₃; Figure S6. (A) Plot of actual and predicted values. (B) Normality plot of residuals for TOC removal efficiency (%): (A) R² = 0.96726 (B) R² = 0.90413; Figure S7. (A) Plot of actual and predicted values. (B) Normality plot of residuals for COD removal efficiency (%): (A) R² = 0.95352 (B) R² = 0.94563; Figure S8. Three-dimensional surfaces of the interaction of independent variables: (A) for GAC and ozone, (B) for current density and GAC, and (C) for current density and ozone in terms of TOC removal efficiency (%); Figure S9. Contour plot of the interaction of the variables: (A) for GAC and current density, (B) for ozone and GAC, and (C) for ozone and current density in terms of TOC removal efficiency (%); Figure S10. Contour plot of the interaction of the variables: (A) for GAC and current density, (B) for ozone and GAC, and (C) for ozone and current density in terms of COD removal efficiency (%); Figure S11. Pareto chart for standardized effects for TOC removal efficiency, $\alpha = 0.05$; Figure S12. Kinetics of TOC and COD removal under optimal conditions; Figure S13. GC/MS spectrum of pharmaceutical wastewater for different treatment processes; Figure S14. Proposed degradation pathway of DMF; Figure S15. GC/MS identification of N-methyl-formamide and formamide as byproducts of DMF; Figure S16. GC/MS mass spectra of N-methyl-formamide and formamide; Figure S17. Degradation pathway of DMAc; Figure S18. BOD₅/COD and toxicity inhibition (%) against COD removal efficiency (%); Figure S19. (A) Changes in acute toxicity (45% basic test). (B) GC/MS spectrum of DMF and its degradation byproducts after 2 h of reaction

Author Contributions: Conceptualization, J.W.G. and R.J.H.T.; methodology, J.W.G. and R.J.H.T.; validation, J.W.G. and R.J.H.T.; formal analysis, J.W.G. and R.J.H.T.; investigation, J.W.G. and R.J.H.T.; writing—original draft preparation, J.W.G. and R.J.H.T.; writing—review and editing, J.W.G., R.J.H.T. and J.H.; supervision, W.W., Z.H., S.L.O. and J.H.; project administration, J.W.G. and J.H. All authors have read and agreed to the published version of the manuscript.

Funding: This research was funded by Singapore Institute of Manufacturing Technology.

Data Availability Statement: Data is contained within the article.

Acknowledgments: The authors would like to thank the financial support from the Simtech research project.

Conflicts of Interest: The authors declare no conflicts of interest.

References

1. Gadipelly, C.; Pérez-González, A.; Yadav, G.D.; Ortiz, I.; Ibáñez, R.; Rathod, V.K.; Marathe, K.V. Pharmaceutical industry wastewater: Review of the technologies for water treatment and reuse. *Ind. Eng. Chem. Res.* **2014**, *53*, 11571–11592. [[CrossRef](#)]
2. Wu, M.; Atchley, D.; Greer, L.; Janssen, S.; Rosenberg, D.; Sass, J. *Dosed Without Prescription: Preventing Pharmaceutical*; Natural Resources Defense Council NRDC Inc.: Washington, DC, USA, 2009.
3. Guo, Y.; Qi, P.S.; Liu, Y.Z. A review on advanced treatment of pharmaceutical wastewater. *IOP Conf. Ser. Earth Environ. Sci.* **2017**, *63*, 012025. [[CrossRef](#)]
4. Shi, X.; Leong, K.Y.; Ng, H.Y. Anaerobic treatment of pharmaceutical wastewater: A critical review. *Bioresour. Technol.* **2017**, *245*, 1238–1244. [[CrossRef](#)]
5. Shi, X.; Lefebvre, O.; Ng, K.K.; Ng, H.Y. Sequential anaerobic–aerobic treatment of pharmaceutical wastewater with high salinity. *Bioresour. Technol.* **2014**, *153*, 79–86. [[CrossRef](#)] [[PubMed](#)]
6. Hu, H.; Jiang, C.; Ma, H.; Ding, L.; Geng, J.; Xu, K.; Huang, H.; Ren, H. Removal characteristics of DON in pharmaceutical wastewater and its influence on the N-nitrosodimethylamine formation potential and acute toxicity of DOM. *Water Res.* **2017**, *109*, 114–121. [[CrossRef](#)]
7. Ji, J.-Y.; Xing, Y.-J.; Ma, Z.-T.; Zhang, M.; Zheng, P. Acute toxicity of pharmaceutical wastewaters containing antibiotics to anaerobic digestion treatment. *Chemosphere* **2013**, *91*, 1094–1098. [[CrossRef](#)] [[PubMed](#)]
8. Bello, M.M.; Raman, A.A.A. Synergy of adsorption and advanced oxidation processes in recalcitrant wastewater treatment. *Environ. Chem. Lett.* **2019**, *17*, 1125–1142. [[CrossRef](#)]
9. Zhan, J.; Li, Z.; Yu, G.; Pan, X.; Wang, J.; Zhu, W.; Han, X.; Wang, Y. Enhanced treatment of pharmaceutical wastewater by combining three-dimensional electrochemical process with ozonation to in situ regenerate granular activated carbon particle electrodes. *Sep. Purif. Technol.* **2019**, *208*, 12–18. [[CrossRef](#)]
10. Wang, T.; Song, Y.; Ding, H.; Liu, Z.; Baldwin, A.; Wong, I.; Li, H.; Zhao, C. Insight into synergies between ozone and in-situ regenerated granular activated carbon particle electrodes in a three-dimensional electrochemical reactor for highly efficient nitrobenzene degradation. *Chem. Eng. J.* **2020**, *394*, 124852. [[CrossRef](#)]

11. Olvera-Vargas, H.; Gore-Datar, N.; Garcia-Rodriguez, O.; Mutnuri, S.; Lefebvre, O. Electro-Fenton treatment of real pharmaceutical wastewater paired with a BDD anode: Reaction mechanisms and respective contribution of homogeneous and heterogeneous OH. *Chem. Eng. J.* **2021**, *404*, 126524. [[CrossRef](#)]
12. Tekle-Röttering, A.; Lim, S.; Reisz, E.; Lutze, H.V.; Abdighahroudi, M.S.; Willach, S.; Schmidt, W.; Tentscher, P.R.; Rentsch, D.; McArdell, C.S.; et al. Reactions of pyrrole, imidazole, and pyrazole with ozone: Kinetics and mechanisms. *Environ. Sci. Water Res. Technol.* **2020**, *6*, 976–992. [[CrossRef](#)]
13. Tekle-Röttering, A.; Jewell, K.S.; Reisz, E.; Lutze, H.V.; Ternes, T.A.; Schmidt, W.; Schmidt, T.C. Ozonation of piperidine, piperazine and morpholine: Kinetics, stoichiometry, product formation and mechanistic considerations. *Water Res.* **2016**, *88*, 960–971. [[CrossRef](#)] [[PubMed](#)]
14. Lewis, D. The absorption spectrum of the titanium (iv)–hydrogen peroxide complex. *J. Phys. Chem.* **1958**, *62*, 1145–1146. [[CrossRef](#)]
15. Elovitz, M.S.; von Gunten, U. Hydroxyl radical/ozone ratios during ozonation processes. I. The Rct concept. *Ozone Sci. Eng.* **1999**, *21*, 239–260. [[CrossRef](#)]
16. von Gunten, U.; von Sonntag, C. *Chemistry of Ozone in Water and Wastewater Treatment*; OAPEN: Pague, The Netherlands, 2012.
17. Yao, C.D.; Haag, W.R. Rate constants for direct reactions of ozone with several drinking water contaminants. *Water Res.* **1991**, *25*, 761–773.
18. Annadurai, G.; Sheeja, R.Y. Use of Box-Behnken design of experiments for the adsorption of verofix red using biopolymer. *Bioprocess Eng.* **1998**, *18*, 463–466. [[CrossRef](#)]
19. Zolgharnein, J.; Shahmoradi, A.; Ghasemi, J.B. Comparative study of Box–Behnken, central composite, and Doehlert matrix for multivariate optimization of Pb (II) adsorption onto Robinia tree leaves. *J. Chemom.* **2013**, *27*, 12–20. [[CrossRef](#)]
20. Nam, S.-N.; Cho, H.; Han, J.; Her, N.; Yoon, J. Photocatalytic degradation of acesulfame K: Optimization using the Box–Behnken design (BBD). *Process Saf. Environ. Prot.* **2018**, *113*, 10–21. [[CrossRef](#)]
21. Wu, C.J.; Hamada, M.S. *Experiments: Planning, Analysis, and Optimization*; Wiley: Hoboken, NJ, USA, 2011; Volume 552.
22. Ferro, S.; De Battisti, A.; Duo, I.; Comninellis, C.; Haenni, W.; Perret, A. Chlorine evolution at highly boron-doped diamond electrodes. *J. Electrochem. Soc.* **2000**, *147*, 2614. [[CrossRef](#)]
23. Scialdone, O.; Galia, A.; Randazzo, S. Electrochemical treatment of aqueous solutions containing one or many organic pollutants at boron doped diamond anodes. Theoretical modeling and experimental data. *Chem. Eng. J.* **2012**, *183*, 124–134. [[CrossRef](#)]
24. Chaplin, B.P. Critical review of electrochemical advanced oxidation processes for water treatment applications. *Environ. Sci. Process. Impacts* **2014**, *16*, 1182–1203. [[CrossRef](#)] [[PubMed](#)]
25. Ganiyu, S.O.; Martínez-Huitle, C.A. Nature, Mechanisms and Reactivity of Electrogenenerated Reactive Species at Thin-Film Boron-Doped Diamond (BDD) Electrodes During Electrochemical Wastewater Treatment. *ChemElectroChem* **2019**, *6*, 2379–2392. [[CrossRef](#)]
26. Zhu, X.; Ni, J.; Xing, X.; Li, H.; Jiang, Y. Synergies between electrochemical oxidation and activated carbon adsorption in three-dimensional boron-doped diamond anode system. *Electrochim. Acta* **2011**, *56*, 1270–1274. [[CrossRef](#)]
27. Georgi, A.; Kopinke, F.-D. Interaction of adsorption and catalytic reactions in water decontamination processes: Part I. Oxidation of organic contaminants with hydrogen peroxide catalyzed by activated carbon. *Appl. Catal. B Environ.* **2005**, *58*, 9–18. [[CrossRef](#)]
28. Turkey, O.; Ersoy, Z.G.; Barışçi, S. The application of an electro-peroxone process in water and wastewater treatment. *J. Electrochem. Soc.* **2017**, *164*, E94. [[CrossRef](#)]
29. Sánchez-Polo, M.; von Gunten, U.; Rivera-Utrilla, J. Efficiency of activated carbon to transform ozone into OH radicals: Influence of operational parameters. *Water Res.* **2005**, *39*, 3189–3198. [[CrossRef](#)]
30. García-Morales, M.A.; Roa-Morales, G.; Barrera-Díaz, C.; Bilyeu, B.; Rodrigo, M.A. Synergy of electrochemical oxidation using boron-doped diamond (BDD) electrodes and ozone (O₃) in industrial wastewater treatment. *Electrochem. Commun.* **2013**, *27*, 34–37. [[CrossRef](#)]
31. Kishimoto, N.; Morita, Y.; Tsuno, H.; Oomura, T.; Mizutani, H. Advanced oxidation effect of ozonation combined with electrolysis. *Water Res.* **2005**, *39*, 4661–4672. [[CrossRef](#)]
32. Qiu, C.; Yuan, S.; Li, X.; Wang, H.; Bakheet, B.; Komarneni, S.; Wang, Y. Investigation of the synergistic effects for p-nitrophenol mineralization by a combined process of ozonation and electrolysis using a boron-doped diamond anode. *J. Hazard. Mater.* **2014**, *280*, 644–653. [[CrossRef](#)]
33. Deshpande, A.M.; Ramakant; Satyanarayan, S. Treatment of pharmaceutical wastewater by electrochemical method: Optimization of operating parameters by response surface methodology. *J. Hazard. Toxic Radioact. Waste* **2012**, *16*, 316–326. [[CrossRef](#)]
34. Garcia-Segura, S.; Ocon, J.D.; Chong, M.N. Electrochemical oxidation remediation of real wastewater effluents—A review. *Process Saf. Environ. Prot.* **2018**, *113*, 48–67. [[CrossRef](#)]
35. Xia, G.; Wang, Y.; Wang, B.; Huang, J.; Deng, S.; Yu, G. The competition between cathodic oxygen and ozone reduction and its role in dictating the reaction mechanisms of an electro-peroxone process. *Water Res.* **2017**, *118*, 26–38. [[CrossRef](#)]
36. Basturk, I.; Murat-Hocaoglu, S.; Varank, G.; Yazici-Guvenc, S. Comparison of Ozonation and Electro-Fenton Processes for Sodium Azide Removal in Medical Laboratory Wastewater by Using Central Composite Design. *Sep. Sci. Technol.* **2021**, *56*, 2951–2966. [[CrossRef](#)]
37. Domínguez, J.R.; González, T.; Palo, P.; Sánchez-Martín, J.; Rodrigo, M.A.; Sáez, C. Electrochemical degradation of a real pharmaceutical effluent. *Water. Air. Soil Pollut.* **2012**, *223*, 2685–2694. [[CrossRef](#)]

38. Chen, Y.; Li, B.; Qiu, Y.; Xu, X.; Shen, S. A novel chemical/biological combined technique for N, N-dimethylformamide wastewater treatment. *Environ. Technol.* **2015**, *37*, 1088–1093. [[CrossRef](#)]
39. Hu, X.; Dong, H.; Zhang, Y.; Fang, B.; Jiang, W. Mechanism of N, N-dimethylformamide electrochemical oxidation using a Ti/RuO₂–IrO₂ electrode. *RSC Adv.* **2021**, *11*, 7205–7213. [[CrossRef](#)] [[PubMed](#)]
40. Kong, Z.; Li, L.; Li, Y.Y. Long-term performance of UASB in treating N, N-dimethylformamide-containing wastewater with a rapid start-up by inoculating mixed sludge. *Sci. Total Environ.* **2019**, *648*, 1141–1150. [[CrossRef](#)] [[PubMed](#)]
41. Cai, S.; Cai, T.; Liu, S.; Yang, Q.; He, J.; Chen, L.; Hu, J. Biodegradation of N-methylpyrrolidone by *Paracoccus* sp. NMD-4 and its degradation pathway. *Int. Biodeterior. Biodegrad.* **2014**, *93*, 70–77. [[CrossRef](#)]
42. Chen, X.; Yang, C.; Wang, W.; Ge, B.; Zhang, J.; Liu, Y.; Nan, Y. Biodegradation of N, N-dimethylacetamide by *Rhodococcus* sp. strain B83 isolated from the rhizosphere of pagoda tree. *J. Environ. Sci.* **2017**, *53*, 88–98. [[CrossRef](#)]
43. Kumar, S.S.; Kumar, M.S.; Siddavattam, D.; Karegoudar, T.B. Generation of continuous packed bed reactor with PVA–alginate blend immobilized *Ochrobactrum* sp. DGVK1 cells for effective removal of N, N-dimethylformamide from industrial effluents. *J. Hazard. Mater.* **2012**, *199*, 58–63. [[CrossRef](#)]
44. Ramirez, F.; Monroy, O.; Favela, E.; Guyot, J.P.; Cruz, F. Acetamide degradation by a continuous-fed batch culture of *Bacillus sphaericus*. In *Biotechnology for Fuels and Chemicals*; Springer: Berlin/Heidelberg, Germany, 1998; pp. 215–223.
45. Bhojani, G.; Jani, S.; Saha, N.K. Facile biodegradation of N, N-dimethylformamide, N, N-dimethylacetamide and N-methyl-2-pyrrolidone by source-derived *Bacillus* strain APS1 for water reclamation and reuse. *J. Clean. Prod.* **2022**, *334*, 130098. [[CrossRef](#)]
46. U.S. Department of Health and Human Services Food and Drug Administration. *Q3C-Tables and List Guidance for Industry*; U.S. Food and Drug Administration: Washton, DC, USA, 2017; p. 7.
47. Byrne, F.P.; Jin, S.; Paggiola, G.; Petchey, T.H.M.; Clark, J.H.; Farmer, T.J.; Hunt, A.J.; McElroy, C.R.; Sherwood, J. Tools and techniques for solvent selection: Green solvent selection guides. *Sustain. Chem. Process.* **2016**, *4*, 7. [[CrossRef](#)]
48. Imamura, S. Catalytic and noncatalytic wet oxidation. *Ind. Eng. Chem. Res.* **1999**, *38*, 1743–1753. [[CrossRef](#)]
49. Groth, G.; Kronauer, K.; Freundt, K.J. Effects of N, N-dimethylformamide and its degradation products in zebrafish embryos. *Toxicol. Vitro.* **1994**, *8*, 401–406. [[CrossRef](#)] [[PubMed](#)]
50. Gescher, A.; Gibson, N.W.; Hickman, J.A.; Langdon, S.P.; Ross, D.; Atassi, G. N-methylformamide: Antitumour activity and metabolism in mice. *Br. J. Cancer* **1982**, *45*, 843–850. [[CrossRef](#)]
51. Scailteur, V.; de Hoffmann, E.; Buchet, J.-P.; Lauwerys, R. Study on in vivo and in vitro metabolism of dimethylformamide in male and female rats. *Toxicology* **1984**, *29*, 221–234. [[CrossRef](#)]
52. Whitby, H.; Gescher, A.; Levy, L. An investigation of the mechanism of hepatotoxicity of the antitumour agent N-methylformamide in mice. *Biochem. Pharmacol.* **1984**, *33*, 295–302. [[CrossRef](#)] [[PubMed](#)]
53. Borenfreund, E.; Shopsis, C. Toxicity monitored with a correlated set of cell-culture assays. *Xenobiotica* **1985**, *15*, 705–711. [[CrossRef](#)]
54. Kennedy, G.L.; Short, R.D. Biological effects of acetamide, formamide, and their monomethyl and dimethyl derivatives. *CRC Crit. Rev. Toxicol.* **1986**, *17*, 129–182. [[CrossRef](#)]
55. Villacorte, L.O. Liquid chromatography–organic carbon detection (LC-OCD). In *Encyclopedia of Membranes*; Springer: Berlin/Heidelberg, Germany, 2014; pp. 1–3.
56. Wirz, K.C.; Studer, M.; Straub, J.O. Environmental risk assessment for excipients from galenical pharmaceutical production in wastewater and receiving water. *Sustain. Chem. Pharm.* **2015**, *1*, 28–35. [[CrossRef](#)]

Disclaimer/Publisher’s Note: The statements, opinions and data contained in all publications are solely those of the individual author(s) and contributor(s) and not of MDPI and/or the editor(s). MDPI and/or the editor(s) disclaim responsibility for any injury to people or property resulting from any ideas, methods, instructions or products referred to in the content.